Research on Laser Target TBM Guidance System Modeling and Intelligent Posture Prediction Algorithms

Xuying Chai[1], Liying Deng[1,*], Yunzhe Gu[2], Shutao Yu[1], Haoqiang Zhang[1]

[1] School of Chemical Equipment, Shenyang University of Technology, Liaoyang 111000, China

[2] Qingdao University of Technology, Qingdao 266000, China

Abstract

In complex geological environments, traditional laser target measurement algorithms face challenges due to multipath effects and spot identification errors, significantly impacting measurement accuracy. This study investigates the optimization of signal processing and spot recognition algorithms for a laser-targeted Tunnel Boring Machine (TBM) guidance system. Utilizing Halcon software for spot image processing and conducting MATLAB simulations, the research verifies the accuracy of position and attitude calculations of the laser target during the TBM digging process. Additionally, an Adaptive Neuro-Fuzzy Inference System (ANFIS) is introduced to predict thrust adjustment requirements for shield attitude control, considering multiple influencing factors. The results indicate that the coordinate deviation of the TBM cutter center was maintained within ±20 mm, meeting the design requirements, and the ANFIS model demonstrated strong learning capabilities in attitude control. These findings offer innovative ideas and methods to enhance the construction accuracy and efficiency of TBM guidance systems, addressing the limitations of traditional measurement techniques.

Keywords

Laser Guidance System; Mathematical Modeling; Algorithm Accuracy; Machine Vision; MATLAB Simulation; Adaptive Neuro-Fuzzy Inference System.

1. Introduction

Tunnel Boring Machine (TBM) is a type of large mechanical equipment specially used for underground tunnel excavation[1]. Its design and function make it play a key role in modern tunnel construction, and it is widely used in the construction of urban subways, underground railways, road tunnels and water conservancy projects[2]. The TBM cuts rock and soil with a rotating cutter head and drives continuously along the predetermined tunnel design axis.

The application of a TBM makes underground construction more efficient and economical. However, in order to ensure the design accuracy and structural stability of the tunnel, the TBM needs to accurately track the design axis and control the progress during the excavation process[3]. This presents a serious challenge to the TBM guidance system. Especially under long-distance or complex geological conditions, traditional guidance systems may have difficulty metting the needs of high precision and high stability. Therefore, the research and improvement of the TBM guidance system, especially its pose measurement algorithm, is very important for improving the construction accuracy and efficiency of the TBM. Wu Xinze[4] compared and discussed the level method, fitted circle center method, three-point method and reference point method in TBM attitude measurement, and verified that the reference point method is more reliable than the other three attitude measurement methods and is suitable for the whole construction stage. Huang Junjie[5] proposed a method based on the

 Volume 11 Issue 2, 2025
DOI: 10.6919/ICJE.202502_11(2).0011

Kalman filter to predict and compensate for observation points to improve the measurement accuracy. Compared with the traditional prism method used to measure the TBM attitude, this method solves the problem of asynchronous attitude measurement via the prism method. Although the guidance system of a TBM has been extensively studied, especially in the application of a laser target system, some progress has been made, but research on the internal component model of a laser target and its application principle is still relatively limited. Most of the research has focused on the performance optimization and system integration of laser targets, but systematic discussions on the accuracy calculation and algorithm of laser target guidance systems are relatively scarce. Therefore, improving the modeling accuracy and algorithm stability of laser target TBM guidance systems is still the focus and challenge of current research.

The purpose of this paper is to discuss a new modeling and pose measurement algorithm for a laser target TBM guidance system, propose an improved algorithm model, and systematically analyze its accuracy. In this work, the vision software Halcon is used to calculate the spot center coordinates of the laser target, which is applied in engineering practice. MATLAB software is used to simulate the attitude data in the driving process of -7~400 rings, compare the actual collected data with the coordinate deviation value of the theoretical model, verify the correctness of the TBM pose precision solution method proposed in this paper, and hopefully provide new ideas and methods to improve the accuracy and stability of the TBM guidance system.

2. Principle Analysis of the Laser Guidance System

Figure 1 shows the scene diagram and main components of the laser steering measurement system. The system includes a total station, laser target, control box, rear-view prism group, industrial computer, radio station and cable, etc. After the two radio stations are paired, the measurement information of the total station can be transmitted to the control box, which is connected to the industrial computer through the network cable, and the data are displayed on the guidance software to control the total station to measure the three-dimensional coordinates of the laser target in real time[6]. The core reference point of the guidance system is a total station with an automatic target recognition (ATR) function[7], which is fixed on the upper right (or upper left) bracket of the tunnel forming segment[8], and the laser target is fixed on the upper right (or upper left) of the middle TBM, and is rigidly fixed to the TBM.

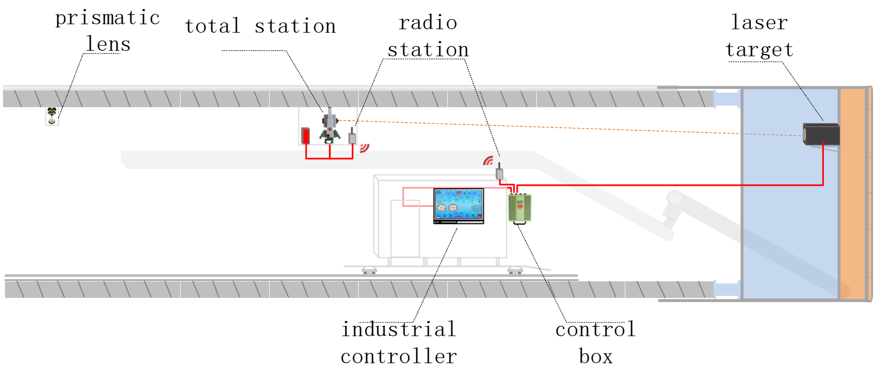

Figure 1. Schematic diagram of the laser guidance system

As the main component of a laser target-type TBM guidance system, the laser target replaces the two forward- looking prisms in the traditional prism TBM guidance system[9] and integrates the angular cone prism, camera, biaxial inclination sensor and core plate into a laser target housing. The prism guidance measurement system ensures not only that the distance between the two forward-looking prisms is greater than 1.2 meters when the equipment is installed but also that the distance between the front and back of the two forward-looking prisms is greater than 1.2 meters. Moreover, angle sensors need to be installed; that is, three devices are installed on the TBM, each of which needs a

ISSN: 2414-1895 DOI: 10.6919/ICJE.202502_11(2).0011

power supply and communication. Moreover, prism-guided measurement systems are prone to situations in which the prism is blocked, which restricts the application of the a TBM with narrow measurement channels. The laser-guided measurement system has a better visibility distance.

The workflow of the laser-guided measurement system is shown in Figure 2. The camera inside the laser target can sense the imaging position of the incident laser and obtain the position data of the laser target by measuring the corner cone prism on the laser target[10]. At the same time, a biaxial tilt sensor built into the laser target measures its rolling angle and pitch angle[11]. The position information and attitude information of the TBM can be further calculated by using the rigid fixed relationship between the laser target and the TBM.

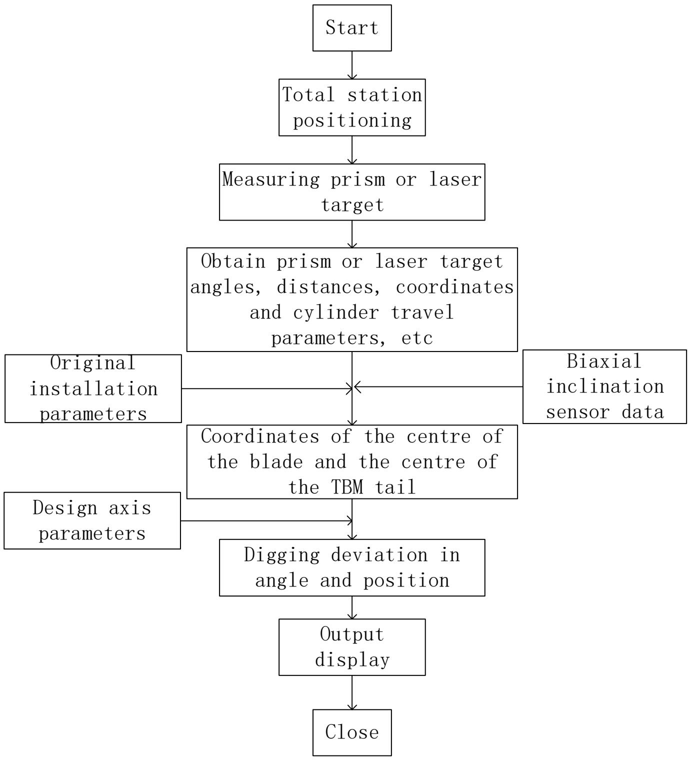

Figure 2. Workflow of the laser guidance system

Figure 3 shows the three-dimensional model of the laser target, and Figure 4 shows the composition structure of the laser target system, including the embedded core plate, biaxial inclination sensor, camera and lens, and corner cone prism. The interaction mechanism between the components is as follows:

First, the angular cone prism is placed in the path of the laser beam. The function of the angular cone prism is to refract the incident laser beam so that it becomes a wider beam[12].

Thus a spot is formed behind it. The camera is then mounted behind the corner prism to capture the resulting spot image. The spot image captured by the camera is transmitted to the embedded core board. The software inside the core board will processes the image to measure the size, shape and position of the spot.

In addition, a biaxial tilt sensor is used to measure the roll angle and pitch angle of the laser target. The sensor is attached to the same rigid body as the camera.Thus, the angle information of the laser target can be obtained through the measurement results of the inclination sensor.

Volume 11 Issue 2, 2025
DOI: 10.6919/ICJE.202502_11(2).0011

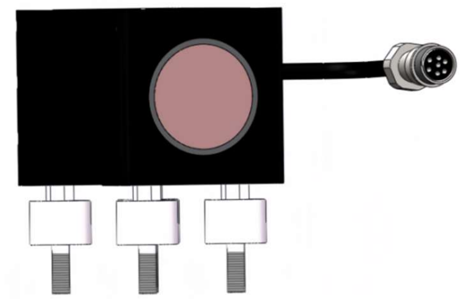

Figure 3. Three-dimensional model of the laser target

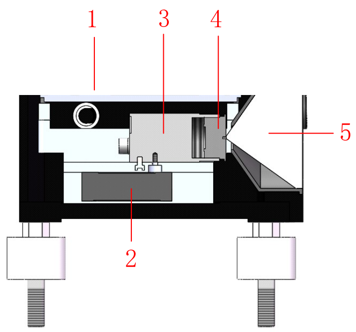

Figure 4. Internal structure of the laser target

1-Laser target embedded core board; 2-Biaxial inclination sensor; 3-Industrial camera; 4-Camera lens; 5-Corner pyramid prism

Through the above steps, the camera placed behind the corner cone prism can effectively measure the spot and incidence angle of the incident laser to calculate the horizontal and vertical positions of the laser target. A biaxial tilt sensor fixed on the same rigid body as the camera can measure the pitch angle and roll angle of the laser target. By combining these data, the attitude and position of the TBM host can be accurately determined, thus improving the alignment accuracy of the laser target and the working effect of the whole system.

3. Analysis of the Working Principle and Mathematical Model of the Internal Components of the Laser Target

3.1 Working Principle and Angle Measurement Technology of the Biaxial Tilt Sensor

3.1.1 Biaxial Inclination Sensor Working Principle

A model diagram of the biaxial inclination sensor is shown in Figure 5. The main purpose of this method is to measure the angle between the biaxial inclination sensor and the horizontal plane of the Earth. The theoretical basis of this method is Newton's second law. When the inclination sensor is stationary, the side and vertical directions have no acceleration effect. The only effect on the inclination meter is gravitational acceleration, and the angle between the vertical axis of gravity and the sensitive axis of the acceleration sensor is the inclination angle[13].

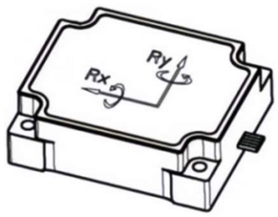

Figure 5. Biaxial inclination sensor model diagram

ISSN: 2414-1895 DOI: 10.6919/ICJE.202502_11(2).0011

The measurement principle of the inclinometer is shown in Figure 6. An object with a mass of m rotates around the horizontal axis, and the rotational angular velocity is $\omega/(rad\cdot s^{-1})$,where L/m is the radius of rotation, $g/(m\cdot s^{-2})$ denotes the acceleration of gravity, and the acceleration of the biaxial tilt sensor can be obtained $a/(m\cdot s^{-2})$.

$$a = g\sin\alpha - \omega^2 L \tag{1}$$

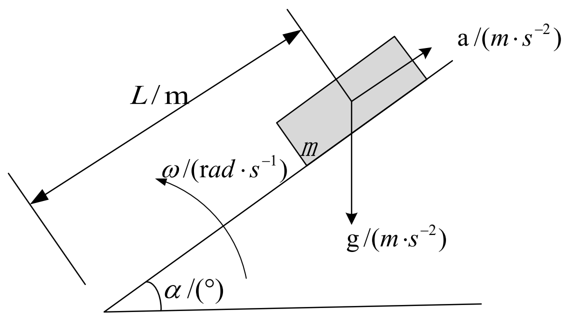

Figure 6. Schematic diagram of the biaxial tilt sensor

3.1.2 Pitch Angle and Roll Angle Measurements

In Figure 7, O_w-$X_wY_wZ_w$ is the world coordinate system, which is used to describe the attitude angle of the object. With the optical center of an industrial camera lens as the origin and the optical axis as the Y axis, a measurement coordinate system O-XYZ is established, where O_R-R_xR_y is the coordinate system of the biaxis inclination sensor. As shown in Figure 8, the pitch angle α is obtained by rotating around the R_x axis, and the rolling angle γ is obtained by rotating around the R_y axis. However, the rolling angle cannot be obtained directly from the measurement value of the axis O_RR_y measured β by biaxial a inclination sensor, because it is related to the pitch angle α.

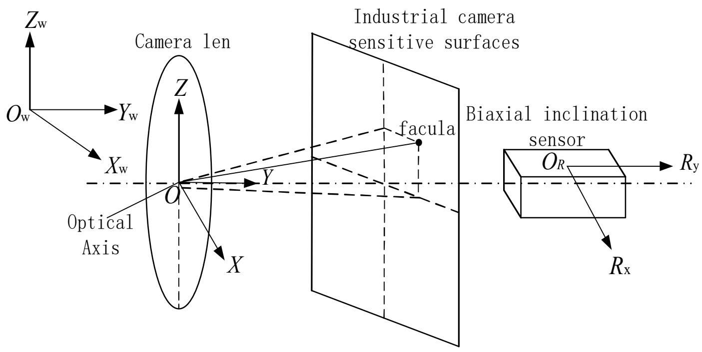

Figure 7. Angle measurement model

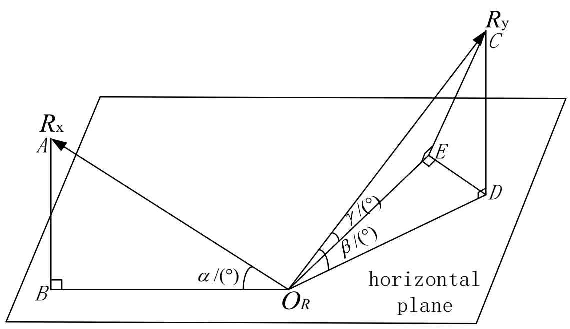

Figure 8. Pitch rolling geometry relation of the biaxial tilt sensor

Volume 11 Issue 2, 2025
DOI: 10.6919/ICJE.202502_11(2).0011

In Figure 8, the letters *A, B, C, D* and *E* represent the intersections of line segments. Since $O_R R_x$ is perpendicular to the plane $O_R CE$, $OB \perp CD$, $OA \perp CE$, $\angle AOB = \angle DCE$, so:

$$\sin\gamma = \frac{CE}{OC}, \sin\beta = \frac{CD}{OC}, \cos\alpha = \frac{CD}{CE} \tag{2}$$

Therefore, the rolling angle γ is:

$$\sin\gamma = \frac{\sin\beta}{\cos\alpha} \tag{3}$$

$$\gamma = \sin^{-1}(\frac{\sin\beta}{\cos\alpha}) \tag{4}$$

The expression formula of the pitch angle and the rolling angle of the biaxial inclination sensor is as follows:

$$\begin{cases} \alpha = \mathrm{a}' \\ \gamma = \arcsin(\frac{\sin\beta}{\cos\alpha}) \end{cases} \tag{5}$$

where a' and β are the measured values of the R_x axis and R_y axis measured by the biaxial inclination sensor.

3.2 Working Principle of the Corner Prism

The angular cone prism is obtained by stretching and cutting the three perpendicular faces of a cube. Therefore, the three reflective surfaces of the angular cone prism are vertical in pairs. The angular cone prism is modeled with SolidWorks, as shown in Figure 9, which shows the rear view, side view and top view of the angular cone prism.

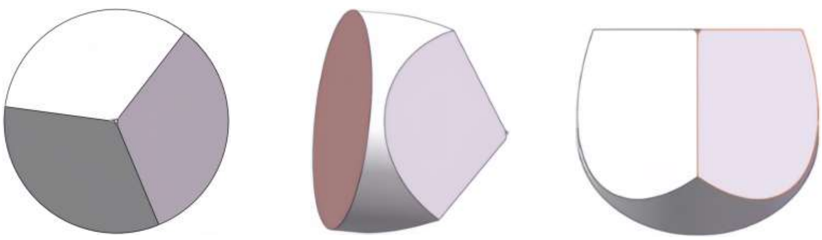

(a)Rear view (b) Side view (c) Top view

Figure 9. Three views of a pyramid prism

The working principle of the angular cone prism is to apply the law of light reflection[14], and its vector diagram is shown in Figure 10. In the figure, *R* is the unit vector of incident light, *F* is the unit vector of reflected light, *N* is the normal unit vector, R_1 is the projection of incident light on the normal line whose direction is downward, R_2 is the projection direction of incident light on the prism interface to the right, F_1 is the projection of reflected light on the normal line whose direction is upward, and F_2 is the projection of reflected light on the prism interface whose direction is right. γ_1, γ_2 are

ISSN: 2414-1895 DOI: 10.6919/ICJE.202502_11(2).0011

respectively the incidence angle and the reflection angle, and the two are equal. The reflected light vector $\vec{F}$ is given by the following formula:

$$\gamma_1 = \gamma_2 \tag{6}$$

$$\vec{R_1} = -|\vec{R_1}|\vec{N} = -(|\vec{R}|\cos\gamma_1)\vec{N} = |\vec{R}|\cos(\pi-\gamma_1)\vec{N} = (\vec{R}\cdot\vec{N})\vec{N} \tag{7}$$

$$\vec{R_2} = \vec{F_2} \tag{8}$$

$$\vec{R_1} = -\vec{F_1} \tag{9}$$

$$\vec{F} = \vec{F_1} + \vec{F_2} = \vec{R_2} - \vec{R_1} = \vec{R} - \vec{R_1} - \vec{R_1} = \vec{R} - 2(\vec{R}\cdot\vec{N})\vec{N} \tag{10}$$

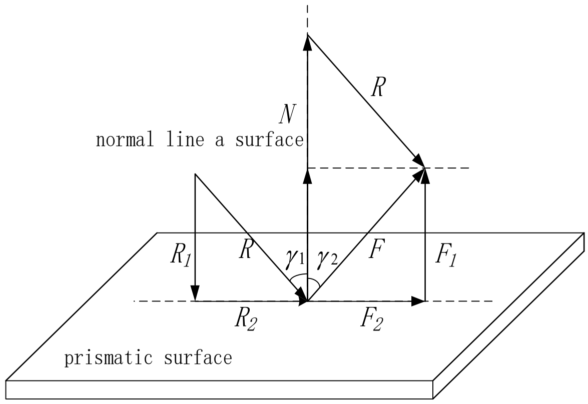

Figure 10. Schematic diagram of light reflection

A space rectangular coordinate system *o-xyz* is established with the three pairwise vertical sides of the pyramid prism. The incident light *R* of the pyramid prism is reflected three times to obtain the fully reflected output light *F*, as shown in the optical path diagram of the pyramid prism in Figure 11. Suppose that the unit normal vectors of the three prism planes are $\vec{N1} = -\vec{\mu}$, $\vec{N_2} = -\vec{\nu}$, $\vec{N_3} = -\vec{\kappa}$ .The reflection characteristics of the corner prism are analyzed.

$$\vec{R} = -x\vec{\mu} - y\vec{\nu} - z\vec{\kappa} \tag{11}$$

After the first reflection, according to equation (10)

$$\vec{F1} = \vec{R} - 2(\vec{R}\cdot\vec{N_1})\vec{N_1} = x\vec{\mu} - y\vec{\nu} - z\vec{\kappa} \tag{12}$$

The second reflection is obtained by combining equations (10) and (12)

$$\vec{F2} = \vec{F1} - 2(\vec{F1}\cdot\vec{N_2})\vec{N_2} = x\vec{\mu} + y\vec{\nu} - z\vec{\kappa} \tag{13}$$

The third reflection is obtained by combining equations (10) and (13)

$$\overrightarrow{F3} = \overrightarrow{F2} - 2(\overrightarrow{F2} \cdot \overrightarrow{N_3})\overrightarrow{N_3} = x\vec{\mu} + y\vec{\nu} + z\vec{\kappa} \tag{14}$$

Therefore, the results verify that the incident ray *R* and the reflected ray *F* are opposite and parallel to each other[15]. After the laser irradiates the corner cone prism, it eventually forms a reflected light spot around the corner cone prism, and this light spot is captured by the camera.

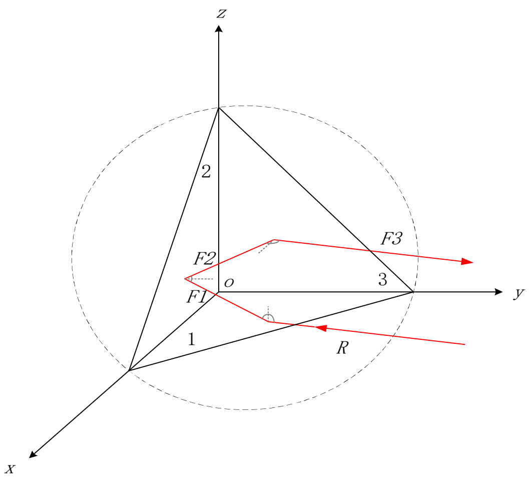

Figure 11. Pyramid prism light path diagram

3.3 Spot Image Processing and Center Positioning based on Halcon

In this work, the algorithm realized camera-taking and image-preprocessing operations by using Halcon, a standard machine vision software developed in Germany[16]. First, the base image and spot image of the same position and exposure time are obtained through the camera. Then, the spot image is preprocessed by denoising and smoothing, and the spot image is subtracted from the bottom image to obtain a new image containing only the brightness information of the spot. Next, the light spot area is separated from the background by threshold segmentation, the position and shape of the light spot are extracted, and the center of gravity of the light spot is calculated to obtain its central coordinates. In this study, by setting the area threshold, the main light spots are screened, and the ghost light spots caused by optical equipment defects are removed[17].

By calculating the weighted average position of the sum of squares of pixels, the central coordinate of the calculated spot can be obtained from formula (18), and the upper left endpoint of the camera coordinate system is the coordinate origin. G_a represents the sum of the gray values of all the pixels in the image, *H(i,j)* represents the gray value of a single pixel, *m* and *n* represents the number of boundary pixels in the selected area of the image, *(i,j)* represent the coordinates of pixels in the image, and *(row,column)* represent the obtained center coordinates of the spot. Figure 12 shows the flow chart for solving the center coordinates of the spot via Halcon. The distance was set to 60 m in the laboratory, and a spot image was taken with an exposure time of 0.03 s. The selected spot profile recognition is shown in Figure 13.

$$G_a = \sum_{i=0}^{m} \sum_{j=0}^{n} H(i,j) \tag{15}$$

$$G_{row} = \sum_{i=0}^{m} \sum_{j=0}^{n} H(i,j)*j^2 \tag{16}$$

$$G_{column} = \sum_{i=0}^{m} \sum_{j=0}^{n} H(i,j)*i^2 \tag{17}$$

$$(row, column) = \left(\sqrt{\frac{G_{row}}{G_a}}, \sqrt{\frac{G_{column}}{G_a}}\right) \tag{18}$$

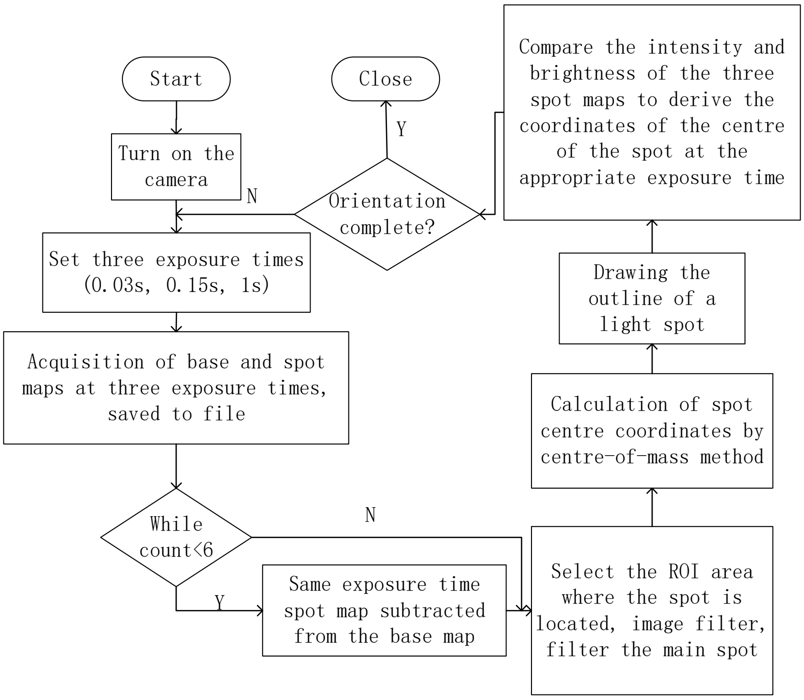

Figure 12. Halcon spot processing flowchart

Figure 13. Spot contour recognition after image preprocessing

4. Mathematical Model of the Laser Guidance Measurement System

4.1 Establishment of the Coordinate System

(1) Geodetic three-dimensional coordinate system. As shown in Figure 14, the Earth's three-dimensional coordinate system takes the due north direction as the *X* axis, the due east direction as

ISSN: 2414-1895 DOI: 10.6919/ICJE.202502_11(2).0011

the Y axis, and the Z axis meets the left-hand coordinate system. This coordinate system is used for the coordinates of the total station and the coordinates of the rear view prism.

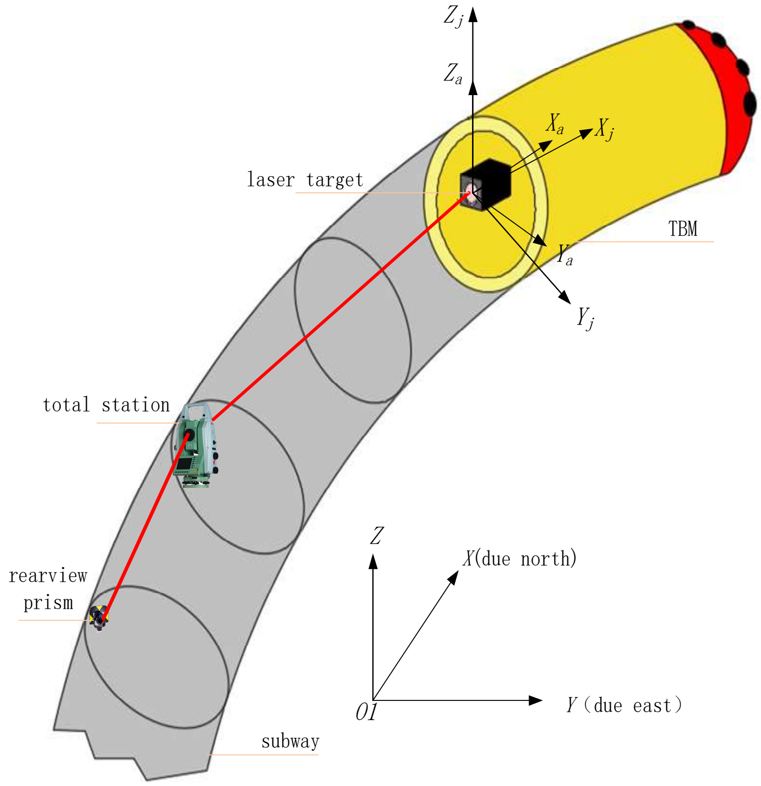

Figure 14. Three coordinate systems in the guiding system

(2) Laser target coordinate system. The laser target is placed horizontally, the origin of the laser target coordinate system is the incision center of the angular cone prism, the positive direction of the X_a axis is the optical center pointing to the center of the laser target rear screen, the Y_a axis is the overoptical center perpendicular to the X_a axis to the right, and the Z_a axis meets the left-hand coordinate system. The rigid zero relation between the laser target coordinate system and the TBM independent coordinate system is determined, including six zero data points, namely, the installation coordinates *a, b, c* of the laser target on the TBM and the angular installation deviation between the two axes $\alpha_0, \gamma_0, \delta_0$.

(3) TBM independent coordinate system. The origin of this coordinate system is the incision center of the corner cone prism, the X_j axis points in the TBM driving direction and is parallel to the TBM axis, the Z_j axis is perpendicular to the laser target facing upward, and the Y_j axis satisfies the left-hand coordinate system. According to the rigidity relationship between the laser target and the initial calibration of the TBM axis position, the center coordinates of the TBM cutter head are determined as shown in Figure 15 and the geometric coordinates of the TBM tail are shown in Equation (19).

$$\begin{cases} \text{TBM cutter centre coordinatesr}: \\ (x_1, y_1, z_1) = (a, -b, -c) \\ \text{Coordinates of the geometric centre} \\ \text{ of the TBM tail}: \\ (x_2, y_2, z_2) = (0, -b, -c) \end{cases} \tag{19}$$

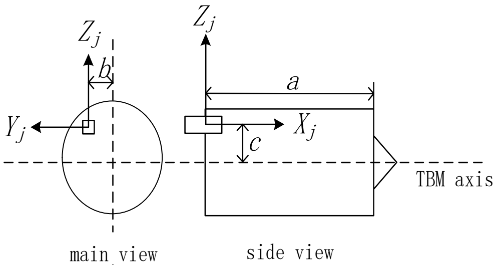

Figure 15. TBM independent coordinate system view

4.2 Solution of the Azimuth Angle of the Laser Target

As shown in Figure 16, the oblique distance *S*, azimuth angle α_1, zenith distance *H*, and *OA* represent the projection of *OX* on the horizontal plane between the total station acquisition and the laser target prism surface. At this time, the horizontal angle α_2 of the photosensitive plane of the laser target is aimed at.

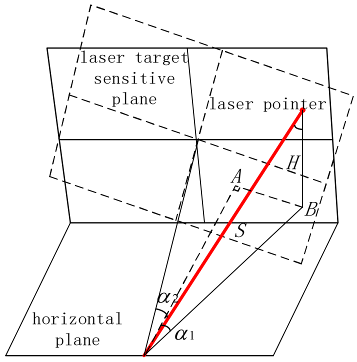

Figure 16. Laser aiming Variable representation of the focal plane of a laser target

The center coordinate of the laser target prism after moving can be calculated via Formula (20), which is the coordinate in the three-dimensional terrestrial coordinate system.

$$\begin{cases} X_a = X_q + S\sin H\cos\alpha_1 \\ Y_a = Y_q + S\sin H\sin\alpha_1 \\ Z_a = Z_q + S\cos H \end{cases} \tag{20}$$

Where X_q, Y_q and Z_q are the coordinates of the total station, and the azimuth of the laser target can be calculated according to the laser point formed on the focal plane of the laser target. As shown in Figure 17, the rolling angle of the laser target is γ, and the pitch angle is α. Then, the azimuth δ is obtained by subtracting the horizontal angle of the laser point irradiated to the photosensitive plane of the laser target α_2 and the azimuth angle of the center of the laser point and the photosensitive plane of the laser target τ.

Where τ is calculated via equation (21), the distance between the camera and the imaging lens is set to 2.8 mm, that is, the distance between the optical center and the center of the photosensitive surface is 2.8mm.

$$\begin{aligned} \tau &= \arctan\left(\frac{\text{Horizontal distance from laser point to photoreceptor centre}}{\text{Horizontal distance from photocentre to photoreceptor centre}}\right) \\ &= \arctan\left(\frac{y\cos\gamma + z\sin\gamma}{0.0028\cos\alpha}\right) \end{aligned} \tag{21}$$

$$\delta = \alpha_2 - \tau \tag{22}$$

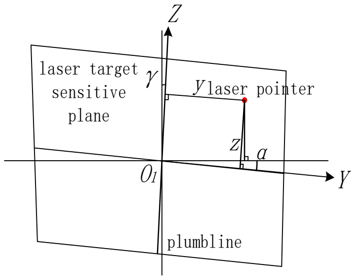

Figure 17. The azimuth angle of the laser target is calculated according to the position of the laser point

4.3 Solving for the TBM Cutter Center and TBM Tail Center Coordinates

Combined with the real-time measurement of the center position coordinates of the laser target prism and the data of pitch angle, roll angle and azimuth angle data, which are programmed as in $X_a, Y_a, Z_a, \alpha, \gamma, \delta$,the six-parameter transformations between the TBM coordinate system and geodetic three-dimensional coordinate system can be solved by referring to the zero data and the six-coordinate parameter conversion method X_a, Y_a, Z_a, A, B, C . Xa, Ya, Za represents the coordinate translation parameters, A, B, C represents the coordinate rotation parameters, $A = \alpha - \alpha_0, B = \gamma - \gamma_0, C = \delta - \delta_0$.

After spatial three-dimensional coordinate conversion, the coordinates of the cutter center and TBM tail center of the TBM are calculated via equation (23). The center coordinate of the cutter head is (X_1, Y_1, Z_1), and the center coordinate of the TBM tail is (X_2, Y_2, Z_2).

$$\begin{bmatrix} X_i \\ Y_i \\ Z_i \end{bmatrix} = R_Z R_Y R_X \begin{bmatrix} x_i \\ y_i \\ z_i \end{bmatrix} + \begin{bmatrix} X_a \\ Y_a \\ Z_a \end{bmatrix} (i = 1,2) \tag{23}$$

The azimuth angle, pitch angle and rolling angle defined in this paper are ZYX normal, so RZ, RY and RX in the formula are rotation matrices around three coordinate axes, as shown in equation (24).

$$R_Z = \begin{bmatrix} \cos\delta & \sin\delta & 0 \\ -\sin\delta & \cos\delta & 0 \\ 0 & 0 & 1 \end{bmatrix}$$
$$R_Y = \begin{bmatrix} \cos\alpha & 0 & \sin\alpha \\ 0 & 1 & 0 \\ -\sin\alpha & 0 & \cos\alpha \end{bmatrix} \tag{24}$$
$$R_X = \begin{bmatrix} 1 & 0 & 0 \\ 0 & \cos\gamma & -\sin\gamma \\ 0 & \sin\gamma & \cos\gamma \end{bmatrix}$$

5. Shield Attitude Control based on Neuro-Fuzzy Inference

Once the center axis of the shield machine deviates from the design trajectory, it leads to attitude deviation, which affects the quality of tunnel boring, and shield attitude control is an important part of shield construction. This deviation may lead to "serpentine" movement of the shield machine. Therefore, the application of artificial neural networks and fuzzy control concepts in attitude control, taking into account the influence of multiple factors, provides an effective reference for shield operators. A shield vertical attitude control model is proposed based on an adaptive Neuro-Fuzzy Inference System (ANFIS).

5.1 Adaptive Neuro-Fuzzy Control Fundamentals

In the field of machinery control, traditional control methods usually start from a structured perspective, search for known laws and impose linear constraints on the controlled object, with a focus on constructing an accurate control model. The adaptive Neuro-Fuzzy Inference System (ANFIS) combines artificial neural networks with fuzzy inference, which compensates for the shortcomings of neural networks in information processing; however, its learning ability is relatively weak, and there is a certain degree of difficulty in accurately capturing the core features of the information.The ANFIS model provides a new concept of shield attitude manipulation through the mutual complementation of the two. Considering that the set of factors affecting the shield attitude selected in this paper contains multiple variables and that vertical attitude control is ultimately achieved through the adjustment of the jack thrust, the control model in this paper adopts the form of one output variable corresponding to multiple input variables, and the ANFIS model generally consists of five layers, which achieves control of the vertical attitude through one output variable corresponding to multiple input variables, as shown in Figure 18.

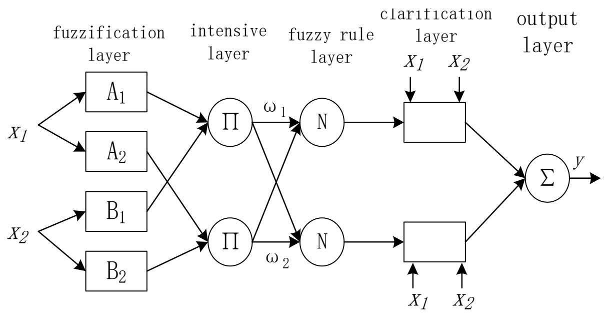

Figure 18. Schematic diagram of the adaptive neuro-fuzzy inference system

As shown in the figure above, the rectangular and circular nodes represent different levels of the neural network structure. The rectangular node represents the adaptive node, where fuzzy and clear values are signaled whereas the circular node, which is capable of directly transmitting the signals and ultimately the expected sample values, is used for regular signal processing.

The relationship between the layers of the structure is as follows: the assumption D_{ji} denotes the output value of node i at the j layer.

(1) Fuzzification layer: This layer is responsible for converting the input explicit values into fuzzy numbers and calculating the corresponding affiliation, which is achieved by selecting an appropriate affiliation function:

$$D_i^1 = \begin{cases} \mu_{A_i}(x_1), i = 1,2 \\ \mu_{B(i-2)}(x_2), i = 3,4 \end{cases} \tag{25}$$

where μ_{A_i}, μ_{B_i} is the degree of affiliation of the input variables in different fuzzy sets.

(2) Reinforcement layer: All the input variables are multiplied to obtain the following result:

$$D_i^2 = \omega_i = \mu_{A_i}(x_i) \times \mu_{B_i}(x_2) i = 1,2 \tag{26}$$

ISSN: 2414-1895 | DOI: 10.6919/ICJE.202502_11(2).0011

(3) Fuzzy planning layer: The normalization calculation is performed on the previous layer of signals:

$$D_i^3 = \varpi = \omega_i / (\omega_1 + \omega_2) i = 1,2 \tag{27}$$

(4) Clarification layer: transforms fuzzy values into clear values:

$$D_i^4 = \varpi_i f_i = \varpi_i (c_0 + c_1 x_1 + c_2 x_2) \tag{28}$$

(5) Output layer: the result of the calculation of the weighted average of the obtained values of the clarification layer:

$$D_i^5 = \sum \varpi_i f_i = \frac{\sum_i \omega_i f_i}{\sum_i \omega_i} \tag{29}$$

5.2 ANFIS-based Attitude Control Models

(1) Control of the input and output variables of the model

The changes in attitude are formed by the existence of a nonlinear mapping with the attitude, which in turn constitutes the joint action of the operator of the attitude control system, the construction environment and the shield equipment. Parameters such as the shield radius, number of cylinders, cutter type, and shield deadweight remain constant and should be removed from the sample set because the data collected in this paper are all from the same construction section and the same shield machine is used. Variables to satisfy the need for attitude control are also added to the offset of the shield pitch angle and the adjustment of the total thrust, and the required variables are detailed in Table 1.

Table 1. Set of input and output variables for the control model

typology	Parameter	unit
input parameter	Pressure on Earth's crust	bar
	Cutter torque	kN.m
	Average speed of advancement	mm/min
	Pitch angle offset	°
output parameter	Total thrust adjustment	N

(2) Attitude control model framework

Combining the principles of the control model and the actual parameter control, the output parameters of the ANFIS model are as follows:

$$\mathrm{y} = \sum_{i=1}^{2} \varpi_i y_i = \sum_{i=1}^{2} \varpi_i (c_0 + c_1 x_1 + c_2 x_2) \tag{30}$$

6. Engineering Experiment and Simulation Verification Analysis

6.1 TBM Driving Trajectory Simulation Experiment

A tunnel project in Xinjiang is taken as a simulation tunnel, and the data generated during TBM tunneling is taken as the actual engineering data. The initial three-dimensional coordinates of the laser target are measured by the total station.The trajectory of the TBM in the -7~400 rings is assumed to be a horizontal straight line, and the trajectory diagram of the three-dimensional coordinates *X*, *Y* and *Z* of the laser target measured in the geodetic coordinate system is shown in Figure 19. Owing to the complex environment in the tunnel, the TBM deviates during the tunneling process, thus affecting the accuracy of the tunneling route. The result is that the trajectory is not a horizontal straight line.

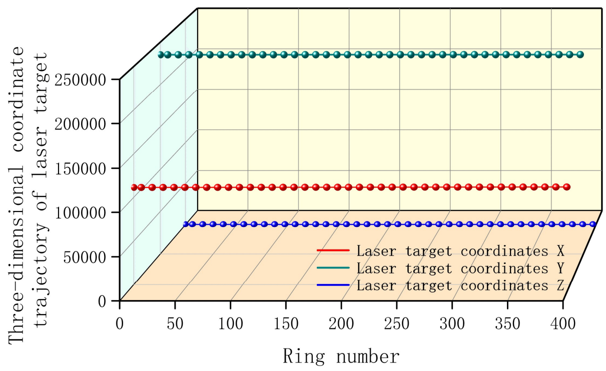

Figure 19. Three-dimensional coordinate trajectory diagram of the laser target

According to the above accuracy calculation method, the deviation between the actual measurement coordinates of the center of the TBM cutterhead and the coordinates of the center of the cutterhead simulated via MATLAB simulation is analyzed, and whether the pose measurement algorithm can meet the requirements of the TBM position and attitude measurement system is determined Table 2 shows the interception of the coordinate data of the actual measurement cutterhead of the -7~400 ring project.

Table 2. Actual measurement cutter center coordinates for the -7~400 ring engineering project

Ring number	Cutter center coordinate X(m)	Cutter center coordinate Y(m)	Cutter center coordinate Z(m)
-7	111675.97	235133.1623	3.3271
50	111750.2745	235175.3814	2.4968
100	111820.7085	235204.9719	0.1981
150	111889.4254	235233.2303	-2.1775
200	111959.11	235261.3881	-4.5329
250	112028.88	235289.5308	-6.8965
300	112098.8312	235317.7198	-9.268
350	112169.0954	235346.0523	-11.6588
400	112237.3366	235373.5876	-13.961

Figure 20 shows the measured TBM cutter head center coordinates *X*, *Y*, *Z* and the *X*, *Y*, *Z* coordinate data line diagram obtained via simulation. The figure shows that the measured coordinates of the actual cutter head center are basically consistent with the simulated coordinate data curve of the algorithm. Owing to the possible measurement errors of the dipmeter, total station and laser point position coordinates (X_a, Y_a, Z_a) and the attitude angle mapping errors of the incident light, there are deviations exist between the actual measured coordinates and the simulated estimated values. However, the *X*- and *Y*- axis errors of the dipmeter are controlled at ±0.0005°, the total station model uses TS16, the angle measurement accuracy reaches 1 ", the ranging accuracy is $(1+1.5\times10^{-6}L)$ mm (L is the measurement distance), and the above deviations are within the accuracy and allowable ranges. In the figure, *Lq1* and *Lq1C* are 1×3 arrays, respectively, representing the center coordinates of the measured cutter head and the simulated cutter head.

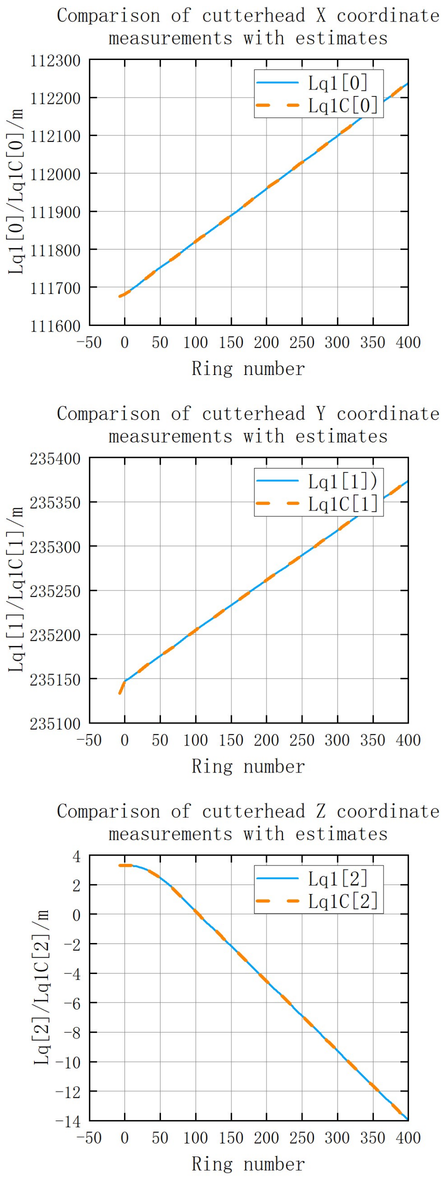

Figure 20. Cutter center measurement coordinates and estimated coordinate curves

According to the measured values of the cutter head center coordinates and the simulated coordinate data, the coordinate deviation can be calculated via equation (31). Figure 21 shows the three-dimensional diagram and three views of the cutter head center deviation of -7~400 rings. The results show that the *X* coordinate deviation of the cutter head center is distributed within ±15mm, the *Y* coordinate deviation is distributed within ±20mm, and the *Z* coordinate deviation is distributed within ±15mm. The positioning accuracy of the large TBM guide system is less than 5cm[18], which meets the position accuracy requirements of the TBM.

 Volume 11 Issue 2, 2025
DOI: 10.6919/ICJE.202502_11(2).0011

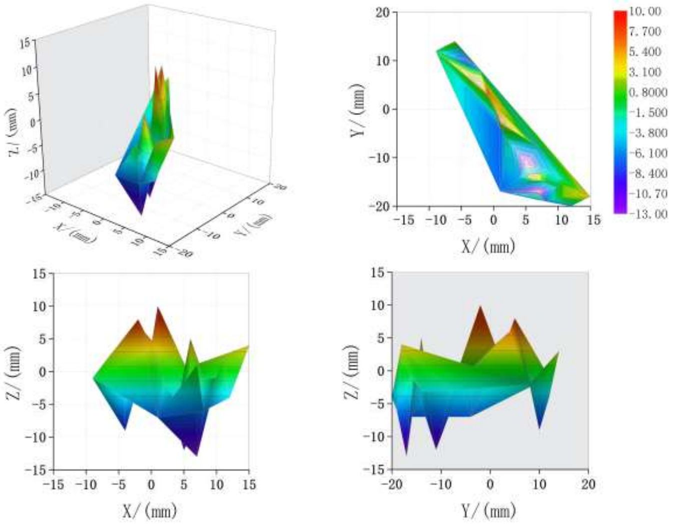

Figure 21. Three-dimensional coordinate diagram of the cutter head center deviation

6.2 Validation of the Shield Attitude Control Prediction

(1) Data input

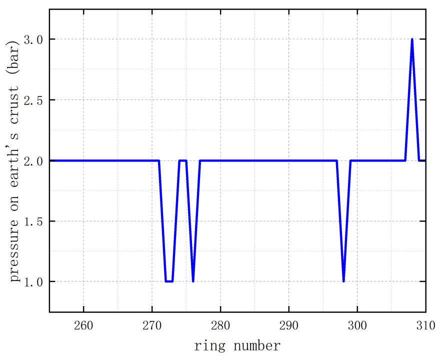

(a) Line graph of soil bin pressure

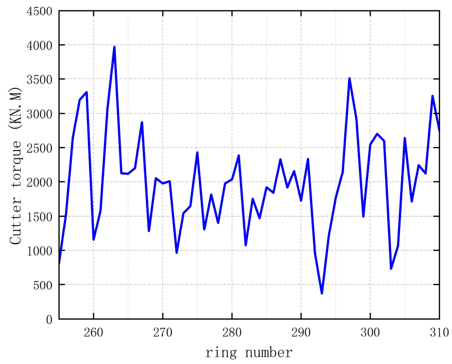

(b) Line graph of torque of cutter disc

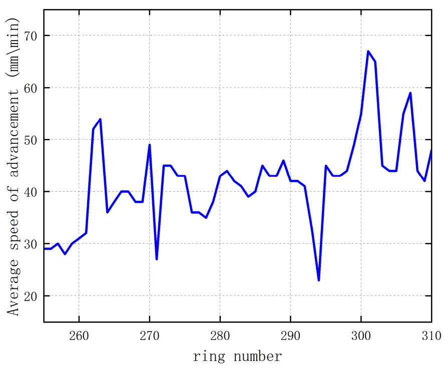

(c) Advancement of average velocity line graphs

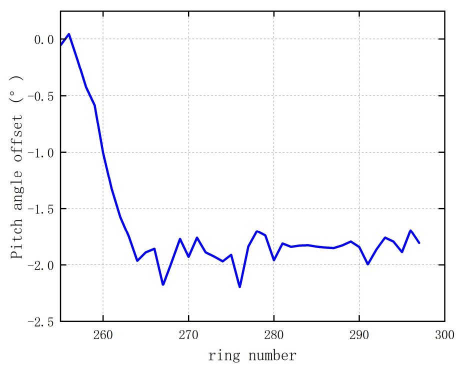

(d) Line graph of pitch angle offset

Figure 22. 255-310 Ring Shield Attitude Control Data Inputs

ISSN: 2414-1895
DOI: 10.6919/ICJE.202502_11(2).0011

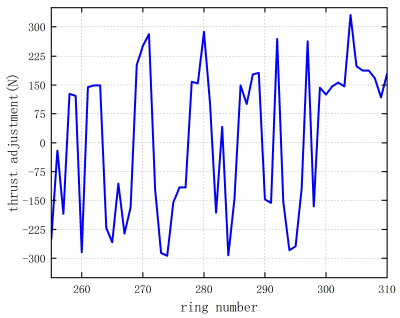

Figure 23. Shield attitude control data output

The input variables of this paper consist of four parameters, including the soil bin pressure, cutter torque and pitch angle offset screened in Section 4.2, while the output variable is the adjusted total thrust. The pitch angle offset is calculated from the simulated data in Section 5.2, which indicates the relative value of the current ring to the previous ring in the shield coordinate system. Since the attitude control in this section performed well, the total thrust adjustment during model training was based on the actual operation of the shield driver. The data of each sample point were collected after the pipe pieces were assembled, and the neighbouring data form rings 255-310 from this section were taken as the sample set as needed. Data preprocessing via the box-and-line diagram method ultimated results in the dataset being imported into the ANFIS attitude control model, as shown in Figure 22 and Figure 23.

The above figure shows that the range of values of various parameters has an influences on the attitude control effect, so it is necessary to control the parameter range when screening the data. The range of the soil chamber pressure is set at 1.0 to 3.0 bar, the torque of the cutter is between 500 and 4000kN.m, the digging speed is between 25 and 70mm/min, the pitch angle deviation is between -2 and 2°, and the adjusted value is distributed in the range of -300 to 300N. Of the 55 rings of data collated, 50 sets were randomly selected as training datasets and the other 5 sets were used as check data sets.

(2)Comparison of results

According to the shield attitude control principle described in Chapter 4, the total target thrust can be calculated, and the thrust adjustment of the next ring obtained through ANFIS model training is added to the actual thrust of that ring. Figure 24 shows the comparison between the raw data of the actual thrust of the next ring and the training results.

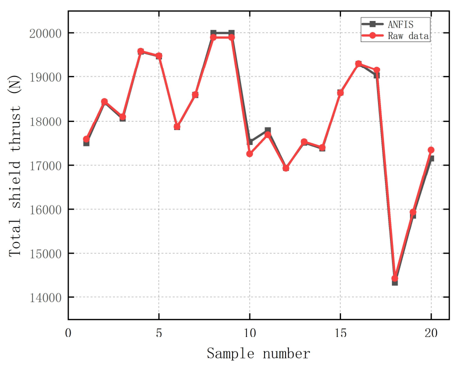

Figure 24. Comparison of the shield attitude control results

The figure above demonstrates the learning capability of the ANFIS method for attitude control of the shield pitch angle. The feasibility of the model can be assessed by determining about the difference between the total shield thrust and the actual value.

7. Conclusion

(1) This paper analyses the working principle of the guidance system and produces a workflow diagram, and explores the interaction mechanism between the internal components of the new laser target.

(2) By analyzing the biaxial inclination sensor, angular cone prism and industrial camera model inside the laser target and its working principle, a mathematical model for the resolution of the spot position of the laser target is established. With the vision software Halcon, an accurate image processing algorithm is applied to calculate the exact coordinates of the spot center, thus achieving continuous capture of the spot and determining the position of the laser point under the optimal exposure time.

(3) In this paper, the attitude control model of an adaptive neuro-fuzzy inference system (ANFIS) is proposed by taking the pitch angle as an example. Neural networks have the ability to self-learn, and fuzzy systems are unique in defining variables, which makes them able to effectively regulate the deviation of the pitch angle. Verified by examples, the ANFIS model shows high accuracy and is suitable for using the historical data of shield construction to speculate the trend of vertical attitude control in the next loop.

(4) A comparison of the between engineering experimental data and MATLAB simulation data reveals that the applied attitude measurement algorithm can control the position deviation within ±20mm within 600m of TBM boring, and the maximum attitude angle error of the laser target is only 0.07°, which is a higher positioning accuracy than that of the conventional guiding system, and is in line with the permissible range of deviation of the position of TBM boring in underground tunnels, which achieves the expected effect.

Acknowledgments

Funding project: Xinjiang National Major Engineering Research Programme Project (EQ075/FY056).

References

[1] Yang X. Application of new technology of full-section tunnel boring machine in coal mine field[J]. Construction Machinery,2024,55(05):88-94+259.

[2] Xi Pan. Application and progress of VMT guidance system for tunnel boring machine[J]. Electronic Testing,2019,(04):93-94+98.DOI:10.16520/j.cnki.1000-8519.2019.04.036.

[3] He Poning. Development and application of automatic guidance system for tunnel boring machine[D]. Central South University,2013.

[4] Wu Xinze, Li Zhongyuan. Comparison of attitude measurement methods of TBM in subway tunnel [J]. Construction Mechanization,2023,44(07):44-46.

[5] Huang Junjie, Zhu Guiguo. Kalman filter should be used in the TBM posture measurement [J]. Journal of east China university of science and technology (natural science edition), 2011, 5 (6) : 82-788. DOI: 10.14135 / j.carol carroll nki. 1006-3080.2011.06.016.

[6] Zhang Mengen. Discussion on laser guidance System of Full Section Boring Machine (TBM) [J]. Mechanical and Electrical Technology of Hydropower Station,2016,39(S1):89-92.DOI:10.13599/ J.CNKI.11-5130.2016.s1.033.

[7] Deng Biao, Huang Teng, Chen Jianhua, et al. 3D accuracy analysis of ATR measured by intelligent total station [J]. Hydropower Automation and Dam Monitoring,2006,(06):57-60.

[8] Gao Shu. Comparative analysis of common TBM total station guidance systems [J]. Modern Tunnel Technology,2015,52(05):200-205.DOI:10.13807/ j.cnki.mtt.2015.05.030.

[9] Meng Xiangrui. Research on key technology of new laser target position measurement system[D]. Tianjin University,2014.

[10] MENG Xiangrui, YANG Xueyou, GAO Yang, et al. Laser target six-degree-of-freedom measurement technique[J]. Optoelectronic Engineering,2015,42(05):27-33.

[11] Shao T. Key technology of laser target for shield attitude measurement[D]. Huazhong University of Science and Technology,2012.

[12] TANG Kai,CHENG Zhi'en,DENG Huarong,et al. Oblique incidence far-field diffraction pattern of angular conical prisms[J]. Physics Letters,2021,70(15):51-60.

[13] CAO Jian-an, ZHANG Le-ping, WU Hao, et al. Research on the analytical method of spatial rotation angle measurement using inclination sensor[J]. Journal of Xi'an Jiaotong University,2013,47(10):109-114.

[14] Lin Laibin. Research on Angle Error Measurement System of Angular Cone Prism [D]. Huazhong University of Science and Technology,2007.

[15] Li D, Liu LY. Effect of Gaussian beam angle error on intrinsic mode polarisation loss in a fully reflective prismatic resonant cavity[J]. Physics and Engineering,2024,34(02):115-119+126.

[16] Guo Haixin, GAO Zibo, Zhang Chenxi, et al. Technology based on 3 d vision camera calibration and 3 d coordinate extraction [J]. Science and technology and innovation, 2023, (14) : 1-7 + 1 to 1. The DOI: 10.15913 / j.carol carroll nki kjycx. 2023.14.001.

[17] Huang Zhe, ZHAO Shiyi, Zhou Weibin, et al. TBM guide laser target oriented mixed light resistant algorithm study [J]. Journal of instruments and meters, lancet 2022 (04) : 172-181. The DOI: 10.19650 / j.carol carroll nki cjsi. J2109109.

[18] Du Shaojun, Zhang Lin, Huang Shitao, et al. Accuracy Simulation and Analysis of automatic guidance System of Total station/Laser inertial Navigation Combined TBM Machine [C]// China Inertial Technology Society. Proceedings of the Symposium on the Dynamic Development Direction of inertial Technology -- New inertial elements and advanced navigation technology. Beijing space time laser navigation technology co., LTD., 2023:17. DOI: 10.26914 / Arthur c. nkihy. 2023.040798.